On the analysis of time-of-flight spin-echo modulated dark-field imaging data

Sales, M.; Plomp, Jeroen; Bouwman, Wim; Tremsin, Anton S.; Habicht, Klaus; Strobl, Markus

DOI
10.1088/1742-6596/862/1/012026

Publication date
2017

Document Version
Final published version

Published in
Journal of Physics: Conference Series

Citation (APA)
Sales, M., Plomp, J., Bouwman, W., Tremsin, A. S., Habicht, K., & Strobl, M. (2017). On the analysis of time-of-flight spin-echo modulated dark-field imaging data. *Journal of Physics: Conference Series*, *862*(012026), 1-10. Article 862. https://doi.org/10.1088/1742-6596/862/1/012026

On the analysis of time-of-flight spin-echo modulated dark-field imaging data

2017 J. Phys.: Conf. Ser. 862 012026

(http://iopscience.iop.org/1742-6596/862/1/012026)

IOP Conf. Series: Journal of Physics: Conf. Series **862** (2017) 012026 doi:10.1088/1742-6596/862/1/012026

On the analysis of time-of-flight spin-echo modulated dark-field imaging data

Morten Sales,[a;b] Jeroen Plomp,[c] Wim G. Bouwman,[c] Anton S. Tremsin,[d] Klaus Habicht[e] and Markus Strobl[a;f]

[a]Nano-Science Center, Niels Bohr Institute, University of Copenhagen, DK-2100 Copenhagen, Denmark,
[b]Department of Physics, Technical University of Denmark, DK-2800, Kgs. Lyngby, Denmark,
[c]Faculty of Applied Sciences, Delft University of Technology, 2629 JB Delft, The Netherlands,
[d]University of California at Berkeley, Space Sciences Laboratory, Berkeley 94720, California, USA,
[e]Helmholtz-Zentrum Berlin fuer Materialen und Energie GmbH, D-14109 Berlin, Germany, and
[f]European Spallation Source ESS-AB, Science Division, SE-22100 Lund, Sweden.

E-mail: markus.strobl@esss.se

Abstract. Spin-Echo Modulated Small Angle Neutron Scattering with spatial resolution, i.e. quantitative Spin-Echo Dark Field Imaging, is an emerging technique coupling neutron imaging with spatially resolved quantitative small angle scattering information. However, the currently achieved relatively large modulation periods of the order of millimeters are superimposed to the images of the samples. So far this required an independent reduction and analyses of the image and scattering information encoded in the measured data and is involving extensive curve fitting routines. Apart from requiring a priori decisions potentially limiting the information content that is extractable also a straightforward judgment of the data quality and information content is hindered. In contrast we propose a significantly simplified routine directly applied to the measured data, which does not only allow an immediate first assessment of data quality and delaying decisions on potentially information content limiting further reduction steps to a later and better informed state, but also, as results suggest, generally better analyses. In addition the method enables to drop the spatial resolution detector requirement for non-spatially resolved Spin-Echo Modulated Small Angle Neutron Scattering.

1. Introduction

While Spin-Echo Small Angle Neutron Scattering (SESANS) [1] is an established small angle neutron scattering technique (SANS) extending the range of SANS to very small (V-SANS) and ultra small (USANS) angles, Spin-Echo Modulated Small Angle Neutron Scattering (SEMSANS) has been introduced only recently [2,3] based on spatial beam modulation induced by spin-echo as proposed and proven earlier [4-6]. SEMSANS can be seen as a variation of SESANS, using less precession regions and providing the option to place the sample behind the spin-manipulation region, hence in a field free region where also magnetic samples can be measured. In contrast to SESANS, not the final beam polarisation, but a spatial beam modulation is measured and analysed, the damping of which provides the same information content as a SESANS polarisation measurement (2,3,7,8). While for SEMSANS a spatially resolved detection is required, it offers on the other hand the potential for spatially resolved SANS studies in an imaging configuration, because the sample can be placed close to the detector and in both techniques a reasonable beam

divergence can be used, allowing for a useful field of view for imaging in SEMSANS [8]. In fact, with the spatially modulated intensity on the detector, SEMSANS resembles the highly successful method to measure dark-field images (DFI) with grating interferometers in neutron imaging instruments [9]. It has been shown recently that both methods are equivalent to SESANS in their capability to measure quantitative small angle scattering [7]. However, the higher fexibility of the magnetic field set-up of SEMSANS in contrast to a grating set-up, which is optimised for a single wavelength, makes SEM-DFI much more efficient for quantitative SANS studies with spatial resolution and in particular in a Time-of-Flight (ToF) mode also able to take advantage of modern pulsed spallation sources.

2. SEMSANS

SEMSANS uses inclined field surfaces to map neutron small angle scattering information into the amplitude dampening of a spatially modulated beam [2-6,8]. The final spin rotation angle of polarised neutrons at the detector depends only on the lateral position with respect to the direction of the inclination of the field surfaces when the focusing condition [4]

$B_1L_1=B_2L_2$ eq. 1

is fulfilled, where B1 and B2 and L1 and L2 are the magnetic fields in the triangular precession regions and their respective distances from the detector. Due to the fact that the final precession angle at the detector is independent of the trajectory and origin in the source, this results in a linearly changing final accumulated spin angle across the beam at the detector. Hence, together with a polarisation analyser downstream the field regions, the result is a spatially modulated intensity across the beam at the detector position with a period given by [5]:

$$\zeta = \frac{\pi \tan\theta_0}{c\lambda(B_2 - B_1)}, \quad \text{eq. 2}$$

where c = 4.632x1014 $T^{-1}m^{-2}$, λ the neutron wavelength and θ_0 the inclination angle of the field surface to the optical axis.

Detecting such modulation in a SEMSANS experiment requires the ability of the detection system to resolve the spatial modulation, which is in one direction only. So far this has been achieved by a combination of slits with a scanning mode, [3,10,11], by gratings with corresponding periods (comparable to neutron grating interferometers) [3,10] or with detectors with 2-dimensional spatial resolution [2,8,12]. Modulation periods of reported measurements to date were of the order of millimeters, which can hence still be resolved by neutron imaging detectors [13].

The correlation length or simply the size-parameter probed with such set-up when applied to small-angle scattering can similar to SESANS [1] be given as the Spin-Echo length,

$$\delta^{SE} = \frac{c\lambda^2 L_S(B_2 - B_1)}{\pi \tan\theta_0} = \frac{\lambda L_S}{\zeta}, \quad \text{eq. 3}$$

with L_S being the sample to detector distance.

If a small angle scattering sample is inserted in the beam, it will cause a dampening of the amplitude of the spatial modulation as the scattering function will redistribute intensities between the minima and maxima, which can be described as a convolution of the modulation function with the scattering function [9]. The visibility of the modulated beam is defined as

$V=(I_{max}-I_{min})/(I_{max}+I_{min})$ eq. 4

where $(I_{max}+I_{min})$ provides the transmission of the sample when normalized with the empty beam measurement ($(I_{0max}+I_{0min})$. Hence the normalized visibility V/V_0 is a transmission corrected entity where V (V_0) is the visibility of the spatially modulated signal, I (I_0), with (without) sample in the beam.

The normalised visibility (V/V_0) can then be modeled by a SESANS correlation function, G, according to [7]:

$$\frac{V(\delta^{SE})}{V_0} = \exp\left\{\Sigma t\left[G(\delta^{SE}) - 1\right]\right\} \quad \text{eq. 5}$$

like described analogue for SESANS in Ref. [1,14,15] and for grating interferometry in [7]. Here t is the sample thickness and Σ is the total scattering cross section of the sample, which e.g. for a two-phase system can be given as $\Sigma=\lambda^2(\Delta\rho)^2\phi(1-\phi)\xi$ [14], with Δρ being the scattering length density contrast, ϕ the volume fraction of one phase, and ξ the correlation length perpendicular to the neutron beam in the probed scattering direction, which is across the modulation.

A scan of δ^{SE}, the correlation length parameter probed (eq. 3), is required for quantitative SANS measurements. This can be achieved according to eq. 3 by either scanning wavelength, sample distance or values of the modulation period, e.g. through the magnetic fields B_1 and B_2, which however have to further fulfill the focusing condition (eq. 1) for the modulation. In order to model and fit data directly with the real space correlation function G, they have to be normalized by sample thickness and for ToF experiments utilizing an extended wavelength band by wavelength square, such that the data is of the form

$$\frac{\ln\left[\frac{V(\delta^{SE})}{V_0}\right]}{\lambda^2 t} = \Sigma\left[G\left(\delta^{SE}\right) - 1\right] \quad \text{eq. 6}$$

However, the actual extraction of the modulation parameters and in particular the off-set providing the attenuation contrast and the visibility providing the SANS information is the main challenge for data reduction and analyses. A spin-echo modulated beam does not provide a constant modulation for an extended cross-section of the beam as the echo condition is only perfectly fulfilled in a particular lateral position and can be framed by a decaying curve as an envelope for the maxima and minima of the spatial modulation like it is well known in neutron spin-echo applications. Additionally, data are affected by statistics. Because in SANS experiments samples can be considered homogeneous with regards to the beam cross section there are several possibilities to extract a single V/V_0 value, however. The most consuming analyses method is to model and fit the modulation curves fully, while the available maxima and minima can also be averaged in order to calculate a single averaged visibility value V and V_0, respectively, which is sufficient for such kind of measurement. This is technically also done in case of using an analyser grating, which can be done when the modulation is kept constant in a ToF measurement [12] or in a monochromatic mode [3] and which by a step scan provides a single modulation curve with a non-spatially resolved detector.

3. SEM-DFI

However, the SEMSANS set-up bears the big advantage as compared to SESANS, that it can be applied combined with imaging in a DFI approach [8] in analogy to that with Talbot Lau grating interferometers [9]. This is the case because here the sample can be placed close to the detector with 2-dimensional spatial resolution, which allows spatial correlation, i.e. image resolution, and an extended beam can be applied where the modulation can be analysed locally, due to the large beam divergence enabled by the technique. Hence, a combined application of SEMSANS and imaging requires an imaging detector with significant 2D spatial resolution. In analogy to grating interferometry the SE modulation can then be utilized in a neutron dark-field imaging mode providing an attenuation contrast image and a spatially resolved SAS analyses of the sample, simultaneously probing two different length scale regimes [8,9].

Because in grating interferometry the modulation periods are fixed by the grating geometries and the set-up needs to be optimized for a particular wavelength, it is much less flexible to probe a broad range of correlation lengths than such SEM-DFI approach [16]. However, modulations achieved with grating set-ups are in the range of micrometers and not directly resolved by the detector but by a scan of an anaylser grating within every pixel. Therefore the spatial resolution is decoupled from the modulation resolution and the correlation lengths probed are of the order of around a micrometer.

In the SEM imaging approach however, periods are of the order of millimeters so far and superposed to the real space image of the sample with entangled spatial resolutions of both the modulation, i.e. SANS signal, and the real space attenuation data. Currently achieved SE modulations are probing size ranges of about 20-200nm, but the data reduction requires significantly different strategies. In principle for the attenuation contrast the full spatial resolution at the detector can be utilized, which is defined by the collimation conditions given in terms of the L/D ration, the sample to detector distance d and indeed the spatial resolution of the imaging detector [13]. L denotes the distance of the source, in the case of a pinhole set-up the pinhole, to the sample while D denotes its dimension, and together with d they define the image blur $b=d(L/D)^{-1}$. However, in current data reduction and analyses the extraction of the attenuation contrast also relies on a full period fitting as will be outlined below. The SANS signal in contrast is smeared over ranges of at least the largest modulation period that provides significant SANS signal in terms of modulation damping. This to date limits the spatial resolution of the quantitative SANS information to the order of mm with this technique. This can only be improved by improving the magnetic field technology and achieving shorter correlation lengths δ_{SE} on smaller periods ζ.

The spatial resolution sought in the SANS signal is the only difference between SEMSANS and the corresponding SEM-DFI approach. While for SEMSANS the sample has to be assumed homogeneous, the opposite is the case for SEM-DFI with respect to attenuation, density, structure parameters and sample thickness. Therefore the possible spatial dependencies have to be taken into account in such applications and the visibility V, which could in SEMSANS be averaged over the beam becomes a function of the spatial dimensions across the beam V(x,y), where it is assumed that x constitutes the modulation direction. This in particular complicates the data reduction to pure wavelength dependent attenuation images and the relative visibility images at each $\delta_{SE}(\lambda)$. Up to date a complex and consuming fitting procedure was applied to the images fitting a sine function on approximately one period and assigning the corresponding offset and visibility values for the attenuation and DFI contrast to the central pixel of the fitted range, while shifting this range pixel by pixel across the x-direction of the image, repeating for every row of y. The required binning of images has to be decided beforehand in order to minimize the fitting routine resources, as fitting accumulates to approximately $1x10^6$ sine fits for a standard 1024x1024 pixel image.

4. Novel Data reduction and analyses

Here we introduce a novel approach to this data reduction, which does not only simplify the data extraction significantly, but also enables regaining full spatial resolution for the attenuation in SEM-DFI and has the potential to overcome the requirement for a spatially resolved detection for straightforward SEMSANS applications. This approach takes advantage of the polarized neutrons required for a spin-echo technique, which implies that two separate measurements with opposite initial spins (I↑ and I↓) and hence modulations shifted by a phase difference of π, can be recorded. Consequently the data can first be reduced to an attenuation corrected modulation, which has the potential to provide all required parameters in every single pixel without the requirement for extensive fitting procedures. Defining

$$M(x) = \frac{I\uparrow(x) - I\downarrow(x)}{I\uparrow(x) + I\downarrow(x)} = \frac{2A(x)}{2I} = \frac{(A_{max} - A_{min})sin(\frac{2\pi}{\zeta}x)}{2I} \qquad \text{eq. 7}$$

where x is the lateral direction of modulation. (Note that the dimension of y is ignored here as all operations can be expanded to y without any implications on the procedure.) The transmitted modulation averaged intensity *I*, i.e. the offset parameter required for the attenuation analyses, has the value

$$2I = I\uparrow(x) + I\downarrow(x) = (I\uparrow_0(x) + I\downarrow_0)e^{-\mu t} = 2I_0e^{-\mu t} \qquad \text{eq. 8}$$

which implies that the position independent attenuation $e^{-\mu t}$ in the case of SEMSANS can be extracted straightforwardly without fitting. I_0 is the modulation averaged incident intensity. While this applies to SEMSANS where the sample has to be considered homogeneous and hence the attenuation constant over the field of view, the attenuation can vary even over a single period in the case of SEM-DFI applications. Note that potential variations of the incident intensity do not play a role as they vanish in the normalization of I/I_0 when extracting the attenuation factor.

In contrast to earlier approaches measurements with both initial spin states carry all relevant modulation parameter information for every position x as can be seen in the schematic of figure 1. The only exception are positions where I↑=I↓ and the close proximity of such positions due to statistics, which will be discussed further down.
Otherwise the normalization

$$\frac{I\uparrow(x)+I\downarrow(x)}{I\uparrow_0(x)+I\downarrow_0(x)} = e^{-\mu(x)t(x)} \qquad \text{eq. 9}$$

straightforwardly provides the local attenuation $e^{-\mu(x)t(x)}$ and the normalization

$$\frac{M(x)}{M_0(x)} = \frac{V(x)}{V_0(x)} = \frac{(A_{max}-A_{min})I_0(x)}{(A_{0max}-A_{0min})I(x)} \qquad \text{eq. 10}$$

which however does not overcome the spatial resolution restriction described earlier for the DFI data. In contrast for the attenuation data the conventional geometric resolution calculation holds to a good approximation despite the redistribution of intensity through small angle scattering, because overall the intensity not scattered or scattered within the spatial resolution limit can be assumed dominant in most cases, as is in conventional imaging.

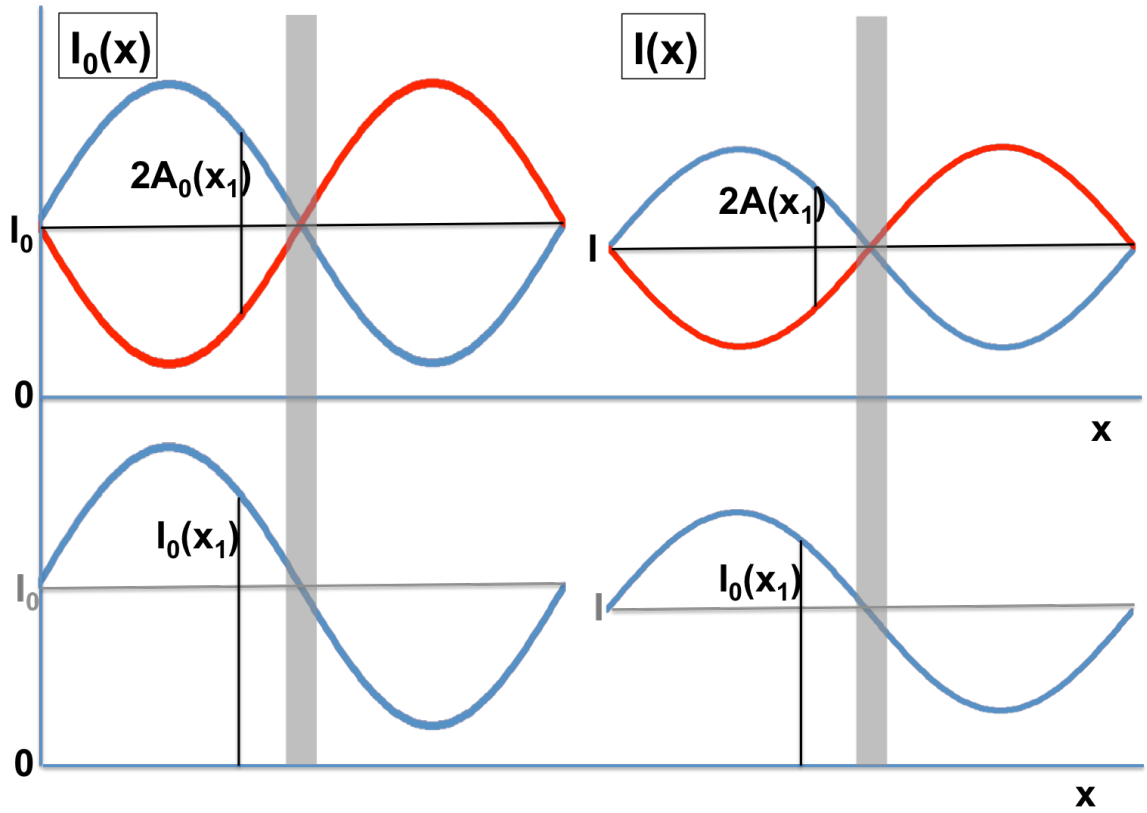

Figure 1. Schematic comparison of information content per pixel utilizing information of spin-up/spin-down measurements (top) versus a conventional single curve approach (bottom). The left side displays schematics of open beam and the right side of a sample measurement, in every case for one period and constant average intensities over such. It becomes obvious that for the top image all information on relative amplitude, i.e. visibility and offset can be extracted for every single point along x independently, while in the bottom example a whole period or a large fraction of it is required to extract such parameterization.

All these operations can be performed straightforwardly as image operations, i.e. by adding, subtracting and dividing the 2D image data. This enables immediate assessment of data and flexible binning at any time in order to improve statistics and assessment. The "blind areas" around I↑=I↓ do not affect SEMSANS measurements without spatial resolution and in DFI imaging mode when done in ToF with changing periods they change with wavelength and hence lead to minor missing sampling in every specific position of an image, certainly beyond spatial resolution for the SANS signal (compare figure 2). Hence they are not an obstacle for data analyses at all.

However, an absolute precondition in order to enable such direct reduction is the phase stability. That means the set-up must enable sufficient stability of the modulation phase all through the measurement of the sample and empty beam.

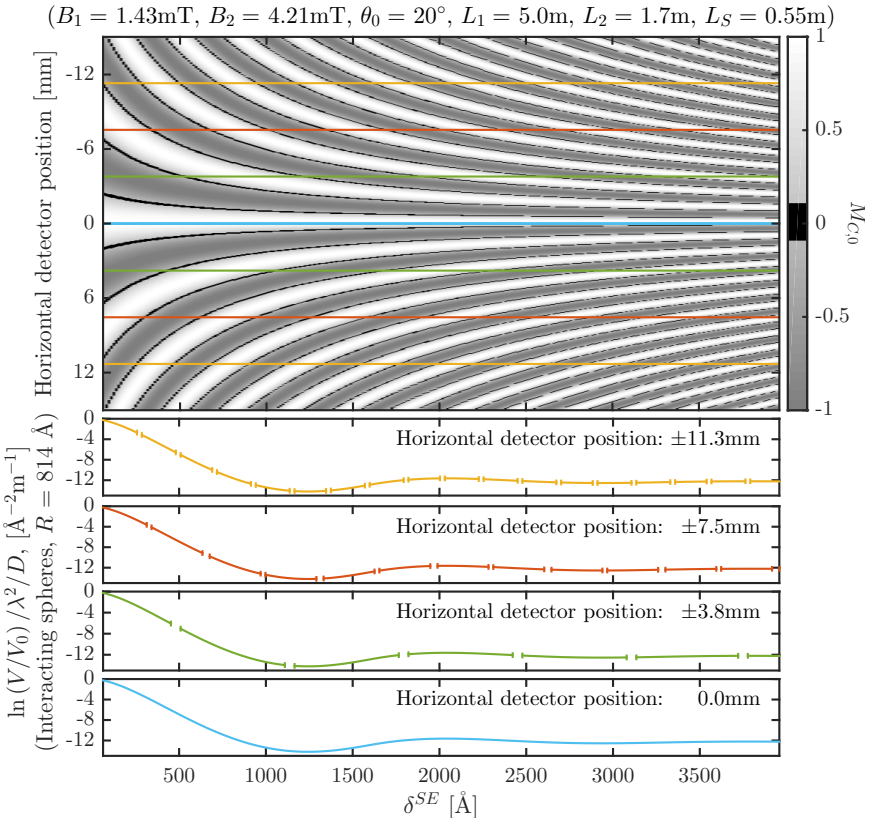

Figure 2. Calculations of scattering curve "dead spots" at different detector positions for a sample of hard spheres in high concentration investigated by SEMSANS using the novel pixel-by-pixel analysis. Each curve corresponds to the signal in a 55 × 55 μm^2 pixel and it can be seen that at the echo position a scattering signal can be extracted for the full Spin-Echo range, whereas at positions away from echo losses of signal occur when M_0 gets close to zero.

5. Measurement and analyses example

Measurements were performed at the Reactor Institute Delft at TU Delft on the SEMSANS setup described in [8], at a thermal source, where the pulsed beam was created using two co-rotating choppers in optically blind mode pro- viding a wavelength resolution of $\delta\lambda/\lambda \sim 5\%$ [17]. The triangular field coils were placed at $L_1 = 5.0$ m and $L_2 = 1.7$ m from the detector, with fields of $B_1 = 1.43$ mT and $B_2 = 4.21$ mT and inclinations angles of $\theta_0 = 20^{\circ}$. Our sample setup, which consisted of a combination of three different sample types, was placed at $L_S = 0.55$ m upstream of the detector. The supermirror multi-channel polariser was oriented so that initial polarisation was vertical whereafter two adiabatic $\pi/2$-rotators were used to choose between spin up or down setting and to rotate the neutron spin into the horizontal plane. Two vertical precession fields were used between polariser and analyser to control the neutron spin and before the analyser a second adiabatic $\pi/2$-rotator pair was used to rotate the neutron spins back to the vertical plane. The supermirror multi-channel analyser was oriented in this plane, such that effects from the structure of the analyser (and polariser) would be perpendicular to the modulation and therefore having no influence on the observed modulation. The Spin-Echo range covered was from about 10 nm to 175 nm. Since our proof-of-principle measurements were performed at a low-flux instrument, we examined three different regions of interest (ROI) covering areas with iron powder, an empty beam area, and dispersed polystyrene colloids in D2O respectively. Each ROI corresponds roughly to a detector area of approximately 50 mm^2 with a detector-pixel size of 55 ×

55 μm^2 [18,19]. Exposure time for every single measurement with spin-up and spin down and with or without samples in the beam was of the order of 3.5 hours, making the total measurement time approximately 14 hours.

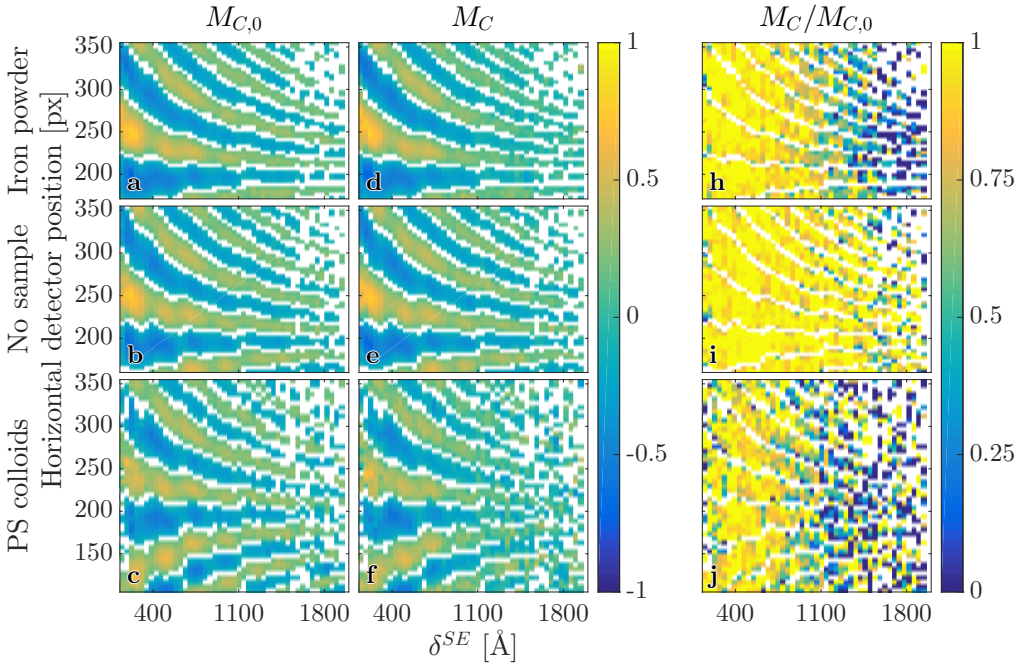

Figure 3. Images a-f show data from the ROIs which has been averaged along the vertical direction on the detector, where the colorscale corresponds to the attenuation corrected modulation and white areas are without information due to either ”dead spots” or low counting statistics. The rows corresponds to the three different sample areas, and images a-c (d-f) are without (with) the sample in the beam. Images h-j show the normalised visibility (eq. 10).

To improve the quality of the obtained images for each Spin-Echo length the images were first filtered using an inverse scale space filter [20] to reduce noise and were averaged over the vertical direction of the ROI, i.e. perpendicular to the modulation direction, which was horizontal. Obviously at an instrument with sufficiently high flux and quality of components the vertical resolution can be as good as the collimation and detector resolution allow. Figure 3 shows the modulation as a function of Spin-Echo length and horizontal detector position. The normalised modulation, $M(x,y)/M_0(x,y)$, was calculated and is shown in figure 3 h-j, where white stripes indicate the positions in time and space with missing information due to the “blind areas” for the DFI signal analyses. As it can be seen in figure 3 h-j (the signal in h and j much faster drops into low visibility regions indicated by green and blue color), and even better in the curves of figure 4, the normalised visibility and the modulation expectedly decrease with increasing Spin-Echo length when there is a small angle scattering sample present. It can also be seen that for long Spin-Echo lengths (long wavelengths) there is a drop in statistics due to the reduced flux of the neutron source at these wavelengths. However, having a higher flux and/or a longer measuring time (possibly in combination with a cold instead of thermal neutron source) will improve statistics and the accessible range of correlations lengths in this regime.

Applying the conventional fitting data analyses for each Spin-Echo length (time frame) and ROI the modulated data in the horizontal detector direction was fitted with a sinusoidal function thereby obtaining the $V(\delta_{SE})$ and V_0 information [8] displayed as the ”sine fitting” curves in

figure 4, where they are compared to curves obtained through our novel approach of dividing the modulation functions achieved by the spin-up and spin-down measurements directly. Reference curves for the three sample types (iron powder, no sample, and polystyrene colloids) are shown as well. Concerning the "blind areas" (figure 2), $V_0 < 0.1$ was set as the threshold for determining their location in order to leave them out of the analyses to avoid corresponding errors due to division by zero. There is a high level of agreement between the curves from the two different reduction methods for data analysis, though at long Spin-Echo lengths the novel approach seems to be more robust with respect to noisier data and shows better precision and better correspondence with the reference curves.

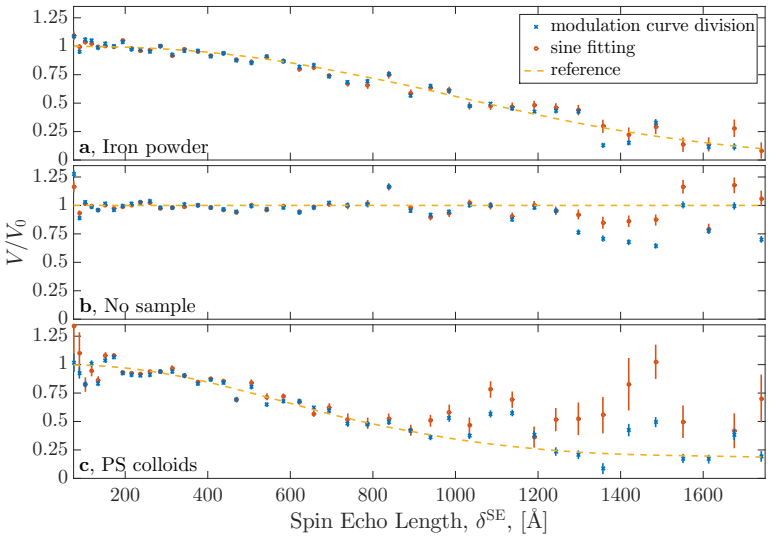

Figure 4. Comparison of relative visibilities dependent on the Spin-Echo length obtained through sine fitting and modulation curve division. The reference curves in a and c are based upon fits of higher resolution SESANS measurements performed individually on the same samples at RID. The model used for the reference curve in a is of a random two-phase media (Andersson et al., 2008) and the model used for the reference curve in c is for hard spheres [21]. For the reference curve in b, V/V_0 is equal to 1 for all Spin-Echo lengths as there is no small angle scattering sample present.

6. Discussion and conclusion

The results clearly demonstrate the feasibility of the approach and its advantages with respect to data reduction effort. It is obvious that the novel strategy enables faster assessment and feedback to measurement and data recording, reduces the resources and increases the flexibility and efficiency for data treatment. It is also demonstrated that the appearance of small blind areas do not affect the data negatively and with respect to the real resolution conditions not at all. Apart from enormous simplification of data treatment in particular for imaging applications the approach would also allow to eliminate the requirement for a high spatial resolution detector or a slit or grating scan for SEMSANS applications. The use of a grating with a duty cycle of about 0.5 and set to the maximum of the spin-up modulation is sufficient for all analyses as all parameters can be extracted for a single sampling position over the modulation. In a ToF approach where the period varies with wavelength in a basic set-up the constant period approach introduced by Sales et al., [12] is suited to overcome that issue. This will in future when higher fields can be realized also enable measurements at very small modulation periods beyond detector resolution limits. In addition such local approach is more robust with respect to altering attenuation over significantly broad periods as well as towards the decay of the modulation amplitude off the echo position. What is, however, maybe even more important overall, is that

this simplified data reduction is significantly more user friendly.

References

[1] Rekveldt M T 1996 *Nucl. Instr. Meth. B* **114** (3-4), 366-370. http://dx.doi.org/10.1016/0168-583X(96)00213-3
[2] Strobl M, Tremsin A S, Hilger A, Wieder F, Kardjilov N, Manke I, Bouwman W G and Plomp J 2012 *J. Appl. Phys.* **112** (1), 014503. http://dx.doi.org/10.1063/1.4730775
[3] Strobl M, Wieder F, Duif C, Hilger A, Kardjilov N, Manke I and Bouwman W G 2012 *Phys. B Condens. Matter* **407** (21), 4132. http://dx.doi.org/10.1016/j.physb.2012.06.036
[4] Gaehler R 2007 *Phys. B* **397** (1-2), 1 200. http://dx.doi.org/10.1016/j.physb.2007.02.034
[5] Bouwman W G, Duif C P and Gaehler R 2009 *Phys. B Condens. Matter* **404** (17), 2585-2589 http://dx.doi.org/10.1016/j.physb.2009.06.052
[6] Bouwman W G, Duif C P, Plomp J, Wiedenmann A and Gaehler R 2011 *Phys. B Condens. Matter* 406(12), 2357-2360. http://dx.doi.org/10.1016/j.physb.2010.11.069
[7] Strobl M 2014 *Sci. Rep.* **4**, 7243. http://dx.doi.org/10.1038/srep07243
[8] Strobl M, Sales M, Plomp J, Bouwman W G, Tremsin A S, Kaestner A, Pappas C and Habicht K 2015 *Sci. Rep.* **5**:16576 | DOI: 10.1038/srep16576
[9] Strobl M, Gruenzweig C, Hilger A, Manke I, Kardjilov N, David C and Pfeiffer F 2008 *Phys. Rev. Lett.* **101** (12), 123902. http://dx.doi.org/10.1103/PhysRevLett.101.123902
[10] Sales, M., Plomp, J., Habicht, K. & Strobl, M. (2015). J. Appl. Crystallogr. **48**(1), 92-96. http://dx.doi.org/10.1107/S1600576714025916
[11] Li F, Parnell S R, Bai H, Yang W, Hamilton W A, Maranville B B,Ashkar R, Baxter D V, Cremer J T and Pynn R 2016 *J. Appl. Cryst.* **49**, 55-63. http://dx.doi.org/10.1107/S1600576715021573
[12] Sales M, Plomp J, Habicht K, Tremsin A, Bouwman W G, Strobl M 2016 *Rev. Sci. Instrum.* **87**, 063907. http://dx.doi.org/10.1063/1.4954727
[13] Strobl M, Manke I, Kardjilov N, Hilger A, Dawson M and Banhart J 2009 *J. Phys. D: Appl. Phys.* **42** 243001 (21pp). doi:10.1088/0022-3727/42/24/243001
[14] Andersson R, van Heijkamp L F, de Schepper I M and Bouwman W G 2008 *J. Appl. Crystallogr.* **41** (5), 868-885.URL: http://dx.doi.org/10.1107/S0021889808026770
[15] Krouglov T, de Schepper I M, Bouwman W G and Rekveldt M T 2003 *J. Appl. Crystallogr.* **36** (1), 117-124. URL: http://dx.doi.org/10.1107/S0021889802020368
[16] Strobl M, Betz B, Harti R P, Hilger A, Kardjilov N, Manke I, Gruenzweig C 2016 *J. Appl. Cryst.* **49** doi:10.1107/S1600576716002922.
[17] van Well A 1992 *Phys. B* **180-181**, 959-961. http://dx.doi.org/10.1016/0921-4526(92)90521-S
[18] Tremsin A, Vallerga J, McPhate J and Siegmund O 2015 Nucl. Instr. Meth. A **787**, 20-25. http://dx.doi.org/10.1016/j.nima.2014.10.047
[19] Tremsin A S 2012 Neutron News **23** (4), 35-38. http://dx.doi.org/10.1080/10448632.2012.725341
[20] Kaestner A, Lehmann E and Stampanoni M 2008 *Adv. Water Resour.* **31** (9), 1174-1187. http://dx.doi.org/10.1016/j.advwatres.2008.01.022
[21] Kinning D J and Thomas E L 1984 *Macromolecules* **17** (9), 1712-1718. http://dx.doi.org/10.1021/ma00139a013